Sphere Fitting as a Check of 3D Imaging System Performance

Marek Franaszek, Geraldine S. Cheok, Kamel S. Saidi, and Christoph Witzgall

Abstract—**Multiple scans of the same object acquired with 3D imaging system (e.g., laser scanner) in the same experimental conditions could provide valuable information about the instrument's performance (e.g., stability, existence of bias, measurement error). Geometrical primitive may be fitted to multiple datasets and the variances of the fitted object's parameters may serve as a measure of instrument's performance. We test this procedure on simulated data as well on the data acquired in a laboratory. Two different error functions (orthogonal and directional) are used to fit a sphere of known radius to the data. A spread of sphere centers fitted with the directional function to simulated data is in agreement with theoretically calculated variances of fitted centers. For sphere centers fitted to the data acquired in a laboratory, the variances do not agree with the spread. This fact is interpreted as an evidence of a non-zero bias in the recorded range data. The orthogonal fitting yields sphere centers in disagreement with theory both for simulated and laboratory datasets.**

Index Terms—**Nonlinear Least Square fitting, 3D imaging systems, experimental noise, orthogonal error function, directional error function.**

I. INTRODUCTION

Current 3D imaging systems may acquire hundreds of thousands of 3D point data within a second [1]. Subsequent processing is often necessary to locate, describe, and identify geometrical objects within those point clouds. One approach is to model an object in terms of parameters that characterize attributes such as location, pose, width, height, etc. [2, 3]. Here, we are working with Nonlinear Least Squares (NLS) fitting methods, based on determining model parameters that minimize a specified error function. A major challenge is how to propagate an instrument error to the errors of fitted parameters. Usually, variances and covariances of fitted parameters are determined from the inverse of the Hessian matrix of an error function. This approach follows from a common practice of linearization of the nonlinear error function near its minimum [4-8].

Among geometric objects, the spheres of known radius R play a special role in a use of 3D imaging systems: sphere center is the only parameter which needs to be determined. In addition, a sphere can be scanned from different directions without any adjustment of the sphere with respect to the instrument. This renders spheres convenient targets to be used in registration of two or more datasets acquired from different instrument positions [9]. It also establishes spheres as unique artifacts for protocol testing the performance of the instrument because the relative distance between two fitted sphere centers can be directly compared with ground truth. In both of these applications, the uncertainty of fitted sphere center has to be established in order to subsequently derive the margins of error for registration as well for deviation from a ground truth.

In our previous reports [10, 11] we investigated two general approaches to fitting as applied to spheres: the orthogonal and the directional fitting methods. We showed there that the orthogonal error function has two minima while the directional error function has only one. In [12] we derived closed formulas needed to calculate variances and covariances of coordinates of sphere centers fitted by minimizing either of these two error functions. Our derivation was more general than the common approach based on a linearization of

an error function around its minimum. We estimated variances directly from sensitivities which, in turn, can be evaluated analytically. The only assumption we make concerns noise level: we assumed that the noise perturbing range measurement is small.

In the current paper we use these closed formulas to check the performance of 3D imaging systems. Specifically, we investigate if tiny bias in range measurement (much smaller than instrument random range error) could be detected. We first check the formulas on spheres fitted to the data generated in computer simulations and then apply the same procedure to the data acquired in a laboratory with a 3D imaging instrument. Results obtained for simulated data show that sphere centers fitted with the directional error function are within the calculated error σ from the truth. Results obtained with the orthogonal error functions applied to the same simulated data show that fitted centers differ from the true center by 3σ or 4σ. For datasets acquired in a laboratory, the true sphere center is not known in the instrument's coordinate system and closed formulas are checked only for repeatability. In the repeatability test, the spread of sphere centers fitted to a few datasets acquired under the same experimental conditions is compared with variances provided by closed formulas. If the spread is less than or equal to the calculated errors for most pairs of sphere centers then the test is passed, otherwise it fails. For almost all datasets acquired in a laboratory and both types of error function, repeatability test failed. This could happen if the instruments used for scanning were collecting range data with systematic small bias. Calculated variances of fitted sphere centers scale as $1/N$ with the number of points in a datasets. Thus, for typical datasets containing hundreds or thousands of points, the resulting variances are very small (usually one or two orders of magnitude below the specified instrument's range error) and therefore they are able to reveal the presence of even small bias in acquired range data.

The paper is organized as follow: in section II we briefly review the derivation of variances of fitted sphere center; in section III two error functions used in minimization are defined; in section IV we outline experiments while in section V we provide the details of numerical calculations. In section VI we present

obtained results followed by discussion in section VII. Final conclusions are presented in section VIII.

II. VARIANCES OF FITTED PARAMETERS

In each of our experiments, a sphere of known radius R, but of presumed unknown center location is fitted to a given point cloud $P_{\{N\}}$. To this end, an error function $Er(U, P_{\{N\}})$ is minimized by varying the model parameters $U = [X, Y, Z]$, which represent a generic sphere center, while keeping the data points $P_{\{N\}}$ = $\{P_j, j = 1,\ldots, N\}$ unchanged. Actual values of P_j are measured in the experiment with N being a number of points in the dataset. For convenience, the dependence of the error function on the radius R will be dropped as it is treated as a constant. Following the Least Squares approach [13-24], each error function considered here is a mean of squares of individual disparities $E_j(U, P_j)$ between "experimental" points P_j and corresponding "theoretical" points:

$$Er(U, P_{\{N\}}) = \frac{1}{N} \sum_{j=1}^{N} E_j^2(U, P_j).$$

(1)

The desired result, the fitted parameters $U^* = [X^*, Y^*, Z^*]$, is then the result of minimizing the error function with respect to the parameters U, with data variables set to represent the experimental data, that is, the actual point cloud at hand. For any admissible point data $P_{\{N\}}$ kept fixed, however, minimizing the error function will produce corresponding parameters

$$U^*(P_{\{N\}}) = \left[X^*(P_{\{N\}}), Y^*(P_{\{N\}}), Z^*(P_{\{N\}}) \right],$$

(2)

which will be considered as functions of $P_{\{N\}}$. For 3D imaging systems, experimental noise predominantly affects the range measurement r_j [25]. The bearings of every experimental point P_j are treated as noise free control variables (φ_j, θ_j) and thus $P_j = r_j [x_j, y_j, z_j]$, where

$$x_j = \cos(\varphi_j)\cos(\theta_j), \quad y_j = \sin(\varphi_j)\cos(\theta_j), \quad z_j = \sin(\theta_j).$$

(3)

In order to calculate the variances of fitted parameters X^*, Y^*, Z^*, we assume no correlations between i-th and j-th measurements (i.e. lack of correlation between measured ranges r_i and r_j). Then, the standard error propagation formula yields the following first order estimates for variances and covariances of fitted sphere

center coordinates [26, 27]

$$\text{var}(X^*) \approx \sum_{j=1}^{N} \left[\frac{\partial X^*(\boldsymbol{P}_{\{N\}})}{\partial r_j} \right]^2 \text{var}(r_j) \,, \tag{4a}$$

$$\text{cov}(X^*,Y^*) \approx \sum_{j=1}^{N} \left[\frac{\partial X^*(\boldsymbol{P}_{\{N\}})}{\partial r_j} \right]\left[\frac{\partial Y^*(\boldsymbol{P}_{\{N\}})}{\partial r_j} \right] \text{var}(r_j) \tag{4b}$$

and similarly for other two components Y and Z. The estimates provided by Equations (4a) and (4b) are generally considered acceptable if the experimental noise of the range measurements r_j is weak, that is, the fitted sphere center remains within a linear domain of response to data perturbation. This requires that, if we were to acquire two point clouds $\boldsymbol{P}_{\{N\}}^{(1)}$ and $\boldsymbol{P}_{\{N\}}^{(2)}$ for the same control variables $\{(\varphi_j,\ \theta_j),\ j = 1,\dots,\ N\ \}$, then the following should hold for two fitted sphere centers

$$\boldsymbol{U}^*\left(\boldsymbol{P}_{\{N\}}^{(2)}\right) \approx \boldsymbol{U}^*\left(\boldsymbol{P}_{\{N\}}^{(1)}\right) + \sum_{j=1}^{N} \frac{\partial \boldsymbol{U}^*\left(\boldsymbol{P}_{\{N\}}^{(1)}\right)}{\partial r_j^{(1)}} \left(r_j^{(2)} - r_j^{(1)} \right) \,. \tag{5}$$

This implies the error of measured range $\sigma(r_j)$ and, consequently, the distance between $\boldsymbol{U}^*(\boldsymbol{P}_{\{N\}}^{(1)})$ and $\boldsymbol{U}^*(\boldsymbol{P}_{\{N\}}^{(2)})$ have to be small in comparison to the sphere radius R.

The coefficients in the Equations (4a) and (4b) represent sensitivities $\partial X^*/\partial r_j$, $\partial Y^*/\partial r_j$ and $\partial Z^*/\partial r_j$. In order to calculate them, we refer to the fact that the vanishing of the gradient – if it exists – is necessary for a minimum to occur. In particular, it follows that substituting the function $\boldsymbol{U}^*\left(\boldsymbol{P}_{\{N\}}\right)$ into the gradient of the error function – with respect to the variables $\boldsymbol{U}$ – vanishes for any admissible data specification. In other words, the vector function

$$\nabla Er\left(\boldsymbol{U}^*\left(\boldsymbol{P}_{\{N\}}\right),\ \boldsymbol{P}_{\{N\}}\right) \equiv 0 \,, \tag{6}$$

which now depends on the variables $\boldsymbol{P}_{\{N\}}$ alone, is identically zero. Differentiation with respect to the range variable r_j produces again an expression which is identically zero, and which according to the chain rule leads to the following 3x3 system of linear equations for every j:

$$H\left(U^*\left(P_{\{N\}}\right), P_{\{N\}}\right) S_j\left(P_{\{N\}}\right) = -V_j\left(U^*\left(P_{\{N\}}\right), P_{\{N\}}\right), \tag{7}$$

where vectors S_j and V_j are defined as

$$S_j\left(P_{\{N\}}\right) = \begin{bmatrix} \dfrac{\partial X^*\left(P_{\{N\}}\right)}{\partial r_j} \\[2mm] \dfrac{\partial Y^*\left(P_{\{N\}}\right)}{\partial r_j} \\[2mm] \dfrac{\partial Z^*\left(P_{\{N\}}\right)}{\partial r_j} \end{bmatrix}, \quad V_j\left(U, P_{\{N\}}\right) = \begin{bmatrix} \dfrac{\partial^2 Er\left(U, P_{\{N\}}\right)}{\partial r_j\, \partial X} \\[2mm] \dfrac{\partial^2 Er\left(U, P_{\{N\}}\right)}{\partial r_j\, \partial Y} \\[2mm] \dfrac{\partial^2 Er\left(U, P_{\{N\}}\right)}{\partial r_j\, \partial Z} \end{bmatrix}. \tag{8a}$$

Matrix H is the hessian of the error function $Er(U, P_{\{N\}})$

$$H\left(U, P_{\{N\}}\right) = \begin{bmatrix} \dfrac{\partial^2 Er}{\partial X^2} & \dfrac{\partial^2 Er}{\partial X\, \partial Y} & \dfrac{\partial^2 Er}{\partial X\, \partial Z} \\[2mm] \dfrac{\partial^2 Er}{\partial Y\, \partial X} & \dfrac{\partial^2 Er}{\partial Y^2} & \dfrac{\partial^2 Er}{\partial Y\, \partial Z} \\[2mm] \dfrac{\partial^2 Er}{\partial Z\, \partial X} & \dfrac{\partial^2 Er}{\partial Z\, \partial Y} & \dfrac{\partial^2 Er}{\partial Z^2} \end{bmatrix}. \tag{8b}$$

Let us note that every element of the matrix H in Equation (8b) contains the sum of N terms, as follows from Equation (1). On the other hand, vector V_j on the right side of Equation (7) contains only one term derived from a given $E_j(U, P_j)$. Therefore, the components of the sensitivity vector S_j must scale as $1/N$ and so do the variance and the covariance of fitted sphere center U^*. The fact that variances of model parameters fitted by Least Squares methods scale as $1/N$ is well known. What is unusual for the fitting procedure discussed in this paper is the magnitude of N: as we mentioned, 3D imaging systems may collect hundreds of thousands of points in a second. Thus, corresponding variances of fitted parameters may become intriguingly small when compared to variances of instrument's measurements. Equations (4a) and (4b) provide general expressions for the variance and covariance of U^*. The particular form of the expressions depends on a choice of an error function used in NLS fitting.

III. SPHERE FITTING

Two error functions were examined in this study: the orthogonal and the directional error function. Their

geometrical meaning is illustrated in Figure 1a. In the orthogonal case, the deviation E_j in Equation (1) is

the distance between the measured point P_j and its orthogonal projection O_j on a sphere surface. The

distance is thus given by

$$E_j^2(U, P_j) = \left(\sqrt{(X - x_j r_j)^2 + (Y - y_j r_j)^2 + (Z - z_j r_j)^2} - R \right)^2 \tag{9}$$

where x_j, y_j, z_j are given by Equation (3). In the directional error function, the deviation E_j is a distance

between P_j and its projection D_j onto the sphere surface along the direction of P_j. If the line from the

instrument through P_j does not intersect the sphere surface, then the point D_j is constructed as in Figure 1b.

Using the following notations:

$$p_j = X x_j + Y y_j + Z z_j, \quad q_j = \sqrt{(y_j Z - z_j Y)^2 + (z_j X - x_j Z)^2 + (x_j Y - y_j X)^2} ,$$

the deviation E_j for the directional error function can be written as

$$E_j^2(U, P_j) = \begin{cases} \left(p_j - \sqrt{R^2 - q_j^2} - r_j \right)^2 & \text{if } q_j < R \\ (p_j - r_j)^2 + (q_j - R)^2 & \text{if } q_j \geq R \end{cases} \tag{10}$$

The quantities p_j and q_j are illustrated in Figure 1b for situations where $q_j \geq R$. Explicit forms for the hessian

matrix H and the vector V_j , needed to solve Equation (7) for sensitivity S_j and ultimately to calculate the

variance and covariance of sphere center, were derived in [12] for the orthogonal and the directional error

function.

IV. EXPERIMENT

Data presented in this paper were collected in a series of experiments. Table I provides the summary of

experimental settings. In total, 87 datasets were collected by scanning four spheres from different distances

and using three different instruments. In some cases, the location of the sphere center was also directly

measured with a total station or a laser tracker for ground truth determination. The first column in Table I

(*Group*) labels six major groups of experiments A-F with further differentiation in some of the groups. All

datasets in a single group were acquired by the same instrument, scanning the same sphere. Within the same

group, different datasets were collected either under the same or different experimental conditions.

Azimuths of sphere centers in subgroup A1 differ from azimuths in A2 by 180°, point clouds in subgroup

D1 were acquired with much higher scanning density than in D2, similarly datasets in subgroups E1-E3

were collected at different scanning densities. Datasets in all groups, except those in subgroups E1-E3, were

acquired for various distances between the instrument and the sphere, respectively. The second column (*#*

Dist) shows the total number of these distances in the given group/subgroup of experiments. The next two

columns (*Min_D* and *Max_D*) provide the smallest and the largest of those distances in meters. The

following two columns (*Min # Points* and *Max # Points*) provide the smallest and the largest number of

points among all datasets in the given group/subgroup.

The next two columns in Table I (*Sphere Type* and *Radius*) indicate which sphere was scanned. There

were four spheres scanned and these spheres were made of different materials, were of different sizes and

had different surface finishes (see Figure 2). Spheres *A* and *B* are made of anodized aluminum, sphere *C* is

made of styrofoam, and sphere *D* is made of titanium. The surface of sphere *C* is rough compared to the

other spheres. Sphere *B* is not a full sphere but a SMR (Spherically Mounted Retroreflector) which allows

its center to be measured with a total station.

The next two columns in Table I (*Instrument Model* and *Err*) indicate the instrument used for scanning

and its range uncertainty in millimeters as specified by the manufacturer. The three instruments used in the

experiments fall into two categories: instrument *In1* has a maximum range of 24 m and range uncertainty on

sub-millimeter level. This instrument is typically used in indoor applications (e.g., in assembly lines in

manufacturing facilities). The other two instruments, *In2* and *In3*, have maximum ranges greater than 100

m and range uncertainty of a few millimeters. They are used in both indoor and outdoor applications (e.g.,

at construction sites).

The next column in Table I (*# Runs*) gives the number of scans acquired under the same experimental

conditions (i.e., the same instrument to sphere distance and scanning density). The column (*Tot # Sets*) is a

multiplication of the second column (*# Dist*) and the column (*# Runs*) and it equals to the total number of datasets for the given group/subgroup.

Finally, the last column (*Alt Instr*) states whether a sphere center was measured with another more accurate instrument: a total station (TS) with a manufacturer specified range error ±0.2 mm or a laser tracker (LT) with measurement error ±30 µm. These precise measurements were obtained in coordinate systems different from the coordinate systems in which the point clouds were acquired (the origin of coordinate system is defined by the location of an instrument: a scanner, a total station or a laser tracker). Therefore, only relative distances between sphere centers fitted to point clouds and those measured directly by the LT or the TS could be compared. All scans were collected indoors under controlled conditions. The points for the sphere in each acquired dataset were manually segmented.

In addition to point clouds acquired with laser scanners in a laboratory, datasets were generated in computer simulations. For a given pair of azimuth and elevation angles (φ, θ), the intersection of a ray from the origin with a hemisphere facing the origin was determined (bearings which did not yield intersections were ignored). The resulting range $r(\varphi, \theta)$ was then perturbed by a small amount obtained from a pseudo random generator of Gaussian noise. The corresponding Cartesian coordinates of the perturbed point were stored for later processing.

V. NUMERICAL CALCULATIONS

A sphere of known radius R was fitted to each dataset using a quasi-Newton minimization procedure [28]. Exit conditions for the optimization process were defined by two parameters, the relative step length and the relative decrease in the value of the error function. Both were set to 10^{-7}. All calculations were performed to double precision on a 32-bit computer. The centroid of the point cloud was selected as a starting point for the minimization. Two different error functions were used: the orthogonal error function (Equation 9) and the directional error function (Equation 10), each of them yielding fitted sphere centers, $\mathbf{U}_o = [X_o, Y_o, Z_o]$ and $\mathbf{U}_d = [X_d, Y_d, Z_d]$, respectively.

In addition to the fitted sphere centers, the variances and covariance of U_o were calculated: $\text{var}(X_o)$, $\text{var}(Y_o)$, $\text{var}(Z_o)$, $\text{cov}(X_o, Y_o)$, $\text{cov}(X_o, Z_o)$, $\text{cov}(Y_o, Z_o)$, and similarly for U_d. These error bounds were calculated from closed forms derived in [12] with the assumption that the bearings (φ_j, θ_j) of the recorded points P_j were determined without errors (i.e., they were treated as control variables) and the only source of experimental error was due to range measurement r_j (φ_j, θ_j). The numerical values of the range errors $\sigma(r_j)$ were chosen according to instrument specifications provided by the manufacturers, as given in Table I, column *Err*.

For each dataset and the corresponding pair of U_o and U_d, a separation distance $\Delta(U_o, U_d)$ was evaluated as $\Delta = F(U_o, U_d)$, where

$$F(U_1, U_2) = \sqrt{(X_1 - X_2)^2 + (Y_1 - Y_2)^2 + (Z_1 - Z_2)^2} \ . \tag{11}$$

The corresponding error of $F(U_1, U_2)$ can be derived from the error propagation formula

$$G(U_1, U_2) = \sqrt{W(U_1, U_2)} / F(U_1, U_2), \tag{12}$$

where

$$W(U_1, U_2) = (X_1 - X_2)^2 (\text{var}(X_1) + \text{var}(X_2)) + 2(X_1 - X_2)(Y_1 - Y_2)(\text{cov}(X_1, Y_1) + \text{cov}(X_2, Y_2)) +$$
$$(Y_1 - Y_2)^2 (\text{var}(Y_1) + \text{var}(Y_2)) + 2(Y_1 - Y_2)(Z_1 - Z_2)(\text{cov}(Y_1, Z_1) + \text{cov}(Y_2, Z_2)) + \tag{13}$$
$$(Z_1 - Z_2)^2 (\text{var}(Z_1) + \text{var}(Z_2)) + 2(Z_1 - Z_2)(X_1 - X_2)(\text{cov}(Z_1, X_1) + \text{cov}(Z_2, X_2)).$$

With this notation, the error of separation distance $\sigma(\Delta) = G(U_o, U_d)$. If the separation distance $\Delta(U_o, U_d)$ is less than its error $\sigma(\Delta)$ then both fitted sphere centers U_o and U_d are considered the same within the statistical error. The ratio $\Delta/\sigma(\Delta)$ shows how the two error functions used in the fitting of a sphere to the same dataset can yield two different sphere centers.

For some groups of experiments, a sphere was scanned more then once in the same experimental settings (column *# Runs* in Table I with entries larger than 1, i.e. subgroups A1, A2, E1-E3 and group B). For these repeated measurements, the spread of the fitted sphere centers and corresponding errors may serve as a useful indicator of the repeatability of the scanning procedure. For each pair (m, n) of datasets collected at a

given sphere to scanner distance, the separation distance $\delta(U_m, U_n) = F(U_m, U_n)$ between the fitted sphere

centers and the corresponding error of separation $\sigma(\delta) = G(U_m, U_n)$ were calculated using Equations (11,12).

The number of different pairs (m, n) available for a single sphere to scanner distance is equal to $K(K-1)/2$,

where K is the number of repeated measurements listed in column *# Runs* in Table I. These calculations

were repeated independently for sphere centers obtained using the orthogonal and directional error function,

yielding δ_O, $\sigma(\delta_O)$ and δ_D, $\sigma(\delta_D)$, respectively. Again, the two fitted sphere centers U_m and U_n are considered

the same within statistical error if the separation distance $\delta(m, n)$ is less than $\sigma(\delta)$. A use of different error

function may yield different result for the same pair (m, n).

For some groups of experiments, the sphere center was measured with other more accurate instruments:

total station or laser tracker (column *Alt Instr* in Table I). Measurements with these instruments were

repeated many times and the mean and standard deviation was recorded for each sphere. The resulting

standard deviations of sphere center locations were at least an order of magnitude smaller than the errors of

sphere centers fitted to point clouds acquired with the 3D imaging systems. These measurements were used

to calculate the relative distances between sphere centers which were later used as the ground truth $GT(m,$

$n)$. For datasets in A1, B, C, and D2, relative distances between fitted sphere centers $D(m, n) = F(U_m, U_n)$

from the same subgroup were calculated together with corresponding errors $\sigma(D) = G(U_m, U_n)$. Then, the

deviations $\varepsilon(m, n)$ from ground truth $GT(m, n)$ were calculated as $\varepsilon(m, n) = D(m, n) - GT(m, n)$. We

assumed no error in the ground truth $GT(m, n)$ and therefore the error of deviation was equal to the error of

a relative distance, $\sigma(\varepsilon) = \sigma(D)$. These calculations were repeated independently for the results from the

orthogonal and the directional fitting, yielding again two pairs of characteristics ε_O, $\sigma(\varepsilon_O)$ and ε_D, $\sigma(\varepsilon_D)$.

Contrary to the laboratory experiments where the location of sphere centers are unknown, the absolute

location of sphere center is known for the simulated datasets. For these datasets only, the deviation $\mu(n)$ of

fitted sphere center U_n from the ground truth and its error $\sigma(\mu)$ were calculated using Equations (11,12)

where n labels different realizations of Gaussian perturbation. Again, these calculations were repeated

independently for the results from the orthogonal and the directional fitting and yielded two sets of

deviations $\mu_O(n)$ and $\mu_D(n)$.

VI. RESULTS

In Figures 3 and 4, typical results from fitting sphere to simulated data are shown. A sphere of radius

$R = 0.0762$ was located at $Q = [19.99, 0.23, 0.02]$ (arbitrary length units, e.g. meters). Nine different

realizations of the Gaussian noise with zero mean and standard deviation equal 0.007 were used to generate

the nine datasets, each containing 1,255 points. Figure 3 shows deviation $\mu(n)$ of fitted sphere center from

Q for the orthogonal and the directional fitting, $n = 1,\dots,9$. Nine noise realizations yield 36 pairs of datasets.

For each pair, the separation δ, its error $\sigma(\delta)$ and the ratio $\delta/\sigma(\delta)$ were calculated. In Figure 4 a histogram of

the ratio is shown for both error functions.

In Figure 5 a similar histogram shows the ratio $\delta/\sigma(\delta)$ calculated for datasets acquired in lab experiments.

Scans repeated in the same settings yield 9 pairs of datasets for A1 subgroup of experiments, 4 for A2, 18

for B, 6 for E1 and E3, and 3 for E2. In total, 46 pairs were used to calculate the ratio $\delta/\sigma(\delta)$ and to create

the histogram shown in Figure 5.

In Figure 6, a histogram of the ratio $\Delta/\sigma(\Delta)$ calculated for all 87 datasets is shown where Δ is a distance

between sphere centers fitted with the orthogonal and the directional error function to the same dataset.

Finally, for groups of experiments A1, B, C, and D2, the deviations $\varepsilon(1, n)$ from ground truth as a

function of relative distance between sphere centers $GT(1, n)$ are shown in Figures (7-10).

VII. DISCUSSION

Histogram in Figure 4 shows that nearly 70 % of all pairs of sphere centers fitted to simulated data with

the directional error have their separation distance δ_D less than corresponding error $\sigma(\delta_D)$ (i.e.,

$\delta_D/\sigma(\delta_D) \leq 1$). The spread of fitted sphere centers agrees with the Gaussian distribution and the directional

fitting passes the repeatability test for datasets perturbed by Gaussian noise. In contrast, datasets acquired in

the laboratory using 3D imaging systems and processed in the same way yield the histogram shown in

Figure 5. This time, the separation distance δ_D is always greater than $\sigma(\delta_D)$. In fact, nearly 70 % of all pairs are large outliers with $\delta_D > 4\sigma(\delta_D)$. It is obvious that repeatability test fails for these datasets. This distinctive disagreement in the performance of the directional fitting applied to simulated and experimental datasets may be due to the fact that the repeatability test assumes that multiple datasets were acquired with a scanner operating in a stable mode, i.e. instrument's parameters were not drifting or slowly oscillating. This assumption becomes especially important when the error of fitted sphere center is much smaller than the range error $\sigma(r_j)$. The assumption could not be independently verified in the performed experiments.

Figure 5 shows that sphere centers fitted to experimental datasets with the orthogonal error function also fail the repeatability test. Only 10 % pairs of the fitted centers have separation distance δ_O less than $\sigma(\delta_O)$ and large outliers constitute almost half of all cases. It is clear that the performance of the orthogonal fitting is equally poor as the directional fitting for datasets acquired in a laboratory. However, for simulated datasets the orthogonal fitting is noticeable different from the directional fitting discussed previously. Figure 4 shows that only 20% of all pairs have the separation distance δ_O less than $\sigma(\delta_O)$, and 40 % of pairs are outliers at a level of $3\sigma(\delta_O)$. In other words, the spread of sphere centers fitted with the orthogonal error is at odds with the Gaussian distribution. Thus, the orthogonal fitting procedure violates the repeatability test for multiple datasets perturbed by stationary Gaussian noise. A possibly different performance of the directional and the orthogonal fitting was already mentioned in [12]. The E_j component of the directional error function is in a form of a deviation between the measured, i.e. noisy quantity r_j and the theoretical quantity $t_j(\boldsymbol{U}_d, \varphi_j, \theta_j)$ which does not depend explicitly on r_j, as in Equation (10). Therefore, vector $\boldsymbol{V}_j$ defined in Equation (8a) does not depend on the measured range r_j. This causes sensitivity vector $\boldsymbol{S}_j$ given by Equation (8a) to be practically independent of r_j for typical datasets (all N measured ranges contribute to the Hessian matrix in Equation (8b) but the influence of an individual r_j is negligible for typical datasets with large N). The j-th component of the orthogonal error function does not have this property and vector $\boldsymbol{V}_j$ as well as the corresponding sensitivity vector $\boldsymbol{S}_j$ depend on r_j. As a consequence, the covariance matrix of

sphere center fitted with the orthogonal error function may be prone to individual random variations in the dataset. The orthogonal fitting of a sphere to range data is an example of more general "non-explicit" regression discussed in [12].

The difference in the performance of the orthogonal and the directional fitting is not limited to the repeatability issue only. Simulated data allow a direct comparison of a fitted sphere center with the ground truth. Deviations $\mu_D(n)$ shown in Figure 3 for nine datasets clearly demonstrate that for most cases μ_D is less than $\sigma(\mu_D)$ for directional fitting and fitted sphere centers are within the statistical error from the true center. For orthogonal fitting, in most cases the deviation μ_O is a few times larger than corresponding error $\sigma(\mu_O)$. In addition, the deviation μ_O is usually a few times larger than the deviation μ_D. This indicates a systematic bias in a location of sphere center introduced by the orthogonal fitting procedure.

For datasets acquired in a laboratory with the 2D imaging systems, a similar comparison between the orthogonal and the directional fitting cannot be done because the true location of sphere center is not known in the instrument coordinate system. Nevertheless, a histogram of the ratio $\Delta/\sigma(\Delta)$ shown in Figure 6 partially supports the conclusion drawn from simulated datasets: fitting a sphere to the same dataset with the orthogonal and the directional error function yield two statistically different centers for most of the processed datasets.

In Figures (7-10) the deviation $\varepsilon(1, n)$ of a relative distance from the corresponding ground truth $GT(1, n)$ is shown. The relative distance $D(1, n)$ between the 1-st and n-th fitted sphere center is calculated and compared with the relative ground truth distance $GT(1, n)$ for experiments A1, B, C, D2. If the deviations from the ground truth were caused by a purely random process, there should be an equal number of deviations with a positive and negative sign. However, the data presented in Figures (7-10) clearly indicate the presence of systematic bias which increases with the relative distance $GT(1, n)$. All deviations ε for datasets acquired with the scanner In1 (subgroup A1) have a positive sign, most deviations for datasets acquired with In2 have a negative sign (groups B and C, subgroup D2). Systematic deviations from ground

truth are seen for both directional and orthogonal fitting. After collecting datasets in experiments C and D, but before B, the scanner In2 was sent to the manufacturer for regularly scheduled maintenance service (discussed here results were not known at the time of service). The regular pattern observed for two different instruments belonging to two different classes reveals the presence of a systematic offset that increases with distance.

The error bars of individual points for the sparse datasets D2 shown in Figure 10 are much larger than corresponding error bars for dense scans A1, C, B shown in Figure (7-9), as predicted by Equations (5) and (7).

VIII. CONCLUSIONS

Fitting sphere to range data with the directional error function is a very sensitive and convenient test of instrument performance. The described procedure is able to generate a single point in 3D space with a very small error, much smaller than the experimental error of individual range measurement. This is due to the fact that modern 3D imaging systems can collect hundreds of thousands of data points within a second and the variances of fitted sphere centers scale as $1/N$ with the number of data points. Thus, even small irregularities in the instrument performance (for example, departure from stationary regime) could be detected.

The comparative study of NLS sphere fitting to range data reveals that the choice of error function for minimization is important. Investigation of two functions, the directional and the orthogonal function, show that the orthogonal fitting should not be used to test the instrument performance. The results obtained for simulated datasets show that orthogonal fitting yields sphere centers systematically different from a true sphere location. This, in turn, causes the spread of fitted centers to be a few times larger than calculated variances of those centers and a failure of repeatability test. Directional fitting yields very different results: sphere centers fitted to the same simulated datasets are within calculated variances from a ground truth and repeatability test is passed.

For datasets acquired in a laboratory, repeatability test fails for sphere centers fitted with the directional error function: the actual spread of fitted centers is four or more times larger than calculated errors. This could happen if the instrument used for scanning introduces a non-zero bias to the collected range data. The bias and associated spread are smaller than the instrument range error. Yet, they can both be detected because variances of sphere centers fitted to the large datasets scale as $1/N$.

Table and Figure Captions

Table I) Summary of experimental settings (see text for details).

Fig. 1) Geometrical interpretation of two error functions used in NLS sphere fitting: P_j is a measured point and O_j is the corresponding theoretical point for the orthogonal fitting. D_j is the corresponding theoretical point for the directional fitting when line-of-sight coming trough P_j: a) intersects with the sphere surface; b) does not intersect.

Fig. 2) Four spheres used in laboratory experiments (after [11]).

Fig. 3) Simulated datasets: comparison of the deviations $\mu(n)$ of the fitted sphere center from the ground truth. The spheres were fitted using the orthogonal and the directional error function. Each deviation $\mu(n)$ has its own error bar determined from Equations (11), (12).

Fig. 4) Simulated datasets: two histograms for orthogonal and direction fitting showing the normalized separation distances $\delta/\sigma(\delta)$ of pairs of sphere centers.

Fig. 5) Lab experiments: two histograms for orthogonal and direction fitting showing the normalized separation distances $\delta/\sigma(\delta)$ of pairs of sphere centers.

Fig. 6) Lab experiments: histogram of the normalized separation distances $\Delta/\sigma(\Delta)$ between sphere centers fitted with the orthogonal and directional error functions to the same datasets.

Fig. 7) Lab experiments, subgroup A1: deviation $\varepsilon(1, n)$ of the relative distance $D(1, n)$ between the first and the n-th fitted sphere center from the corresponding ground truth as a function of $D(1, n)$: a) orthogonal fitting; b) directional fitting. Error bars were determined from Equations (11), (12).

Fig. 8) The same as in Figure 7 but for datasets in group B: a) orthogonal fitting; b) directional fitting.

Fig. 9) The same as in Figure 7 but for datasets in group C. a) orthogonal fitting; b) directional fitting.

Fig. 10)   The same as in Figure 7 but for datasets in subgroup D2: a) orthogonal fitting; b) directional fitting. Large error bars are consequence of low scanning density and small number of data points N.

REFERENCES

[1]   SPAR,   "3D   Imaging   and   Positioning   for   Design,   Construction,   Manufacturing, http://sparllc.com/spar2009.php?page=presentations," 2009.

[2]   F. Bosche and C. T. Haas, "Automated retrieval of 3D CAD model objects in construction range images," *Automation in Construction,* vol. 17, pp. 499-512, 2008.

[3]   S. W. Kwon, F. Bosche, C. Kim, C. T. Haas, and K. A. Liapi, "Fitting range data to primitives for rapid local 3D modeling using sparse range point clouds," *Automation in Construction,* vol. 13, pp. 67-81, 2004.

[4]   A. C. Davidson, *Statistical Models*. Cambridge: Cambridge University Press, 2003.

[5]   N. R. Draper and H. Smith, *Applied Regression Analysis*, 2nd ed. New York: Wiley, 1981.

[6]   D. A. Freedman, *Statistical Models, Theory and Practice*, revised ed. Cambridge: Cambridge University Press, 2009.

[7]   D. M. Himmelblau, *Process Analysis by Statistical Methods*. New York: Wiley, 1970.

[8]   K. Kanatani, *Statistical Optimization for Geometric Computation*. New York: Elsevier, 1996.

[9]   M. Franaszek, G. S. Cheok, and C. Witzgall, "Fast automatic registration of range images from 3D imaging systems using sphere targets," *Automation in Construction,* vol. 18, pp. 265-274, 2009.

[10]   C. Witzgall, G. S. Cheok, and A. J. Kearsley, "Recovering Circles and Spheres from Point Data," in *Perspectives In Operations Research*, F. B. Alt, M. C. Fu, and B. L. Golden, Eds. New York: Springer, 2006, pp. 393-413.

[11]   M. Franaszek, G. S. Cheok, K. S. Saidi, and C. Witzgall, "Fitting Spheres to Range Data from 3D Imaging Systems," *IEEE Trans. Instrum. Meas. ,* 2009 - in print.

[12]   C. Witzgall and M. Franaszek, "Sensitivities and Variances for Fitted Parameters of Spheres " NIST IR 2009.

[13]   S. J. Ahn, W. Rauh, and H. J. Warnecke, "Least-squares orthogonal distances fitting of circle, sphere, ellipse, hyperbola, and parabola," *Pattern Recognition,* vol. 34, pp. 2283-2303, 2001.

[14]   D. Clouse and C. Padgett, "Estimating the position of a sphere from range images " in *Aerospace Conference Proceedings, IEEE*, 2002, pp. 2193-2204.

[15]   I. D. Coope, "Circle Fitting by Linear and Nonlinear Least Squares," *J. Optimization Theory Applicat.,* vol. 76, pp. 381-388, 1993.

[16]   W. Gander, G. H. Golub, and R. Strebel, "Least-squares fitting of circles and ellipses," *BIT,* vol. 34, pp. 558-578, 1994.

[17]   J. Garcia-Lopez, P. A. Ramos, and J. Snoeyink, "Fitting a set of points by a circle," *Discrete and Computational Geometry,* vol. 20, pp. 389-402, 1998.

[18]   B. A. Jones and R. B. Schnabel, "A comparison of two sphere fitting methods.," in *IEEE Proceedings of the Instrumentation and Measurement Technology*, 1986.

[19]   I. Kasa, "A Circle Fitting Procedure and Its Error Analysis," *IEEE Trans. Instrum. Meas.,* vol. 25, pp. 8-14, 1976.

[20]   Y. Nievergelt, "Computing circles and spheres of arithmetic least squares," *Comput. Phys. Commun.,* vol. 81, pp. 343-350, 1994.

[21]   M.   Renault,   "Fitting   Circles   and   Ellipses   to   Data   Using   the   Least-Squares   Method,"   in *http://www.math.temple.edu/~renault/ellipses.html*.

[22]   C. M. Shakarji, "Least-Squares Fitting Algorithms of the NIST Algorithm Testing System," *Journal of Research of NIST,* vol. 103, pp. 633-640, 1998.

[23]   H. Spath, "Least-Square Fitting with Spheres," *J. Optimization Theory Applicat.,* vol. 96, pp. 191-199, 1998.

[24]   D. Umbach and K. N. Jones, "A Few Methods for Fitting Circles to Data," *IEEE Trans. Instrum. Meas. ,* vol. 52, pp. 1881-1885, 2003.

[25]   W. C. Stone, M. Juberts, N. Dagalakis, J. Stone, and J. Gorman, "Performance Analysis of Next-Generation LADAR for Manufacturing, Construction, and Mobility," *NISTIR* vol. 7117, 2004.

[26]   GUM,   "Evaluation   of   measurement   data   -   Guide   to   the   expression   of   uncertainty   in   measurement (http://www.bipm.org/en/publications/guides/gum.html)," JCGM 2008.

[27]   H. Ku, "Notes on the Use of Propagation of Error Formulas," *Journal of Research National Bureau of Standards,* vol. 70C, pp. 331 - 341, 1966.

[28]   W. H. Press, S. A. Teukolsky, W. T. Vetterling, and B. P. Flannery, *Numerical Recipes in C, 2nd Edition*: Cambridge University Press, 1995.

Group	# Dist	Min_D [m]	Max_D [m]	Min # Points	Max # Points	Sphere Type	Sphere R [m]	Instrument Model	Instrument Err [mm]	# Runs	Tot # Sets	Alt Instr
A1	9	4.05	21.19	888	1,199	D	0.0508	In1	0.1	2	18	LT
A2	4	1.72	23.88	1,093	1,196	D	0.0508	In1	0.1	2	8	LT
B	6	15.07	159.91	523	741	B	0.0762	In2	7	3	18	TS
C	7	9.99	99.92	1,096	1,297	B	0.0762	In2	7	1	7	TS
D1	11	10.85	65.84	1,268	3,813	D	0.0508	In2	7	1	11	LT
D2	11	10.85	65.84	13	59	D	0.0508	In2	7	1	11	LT
E1	1	6.26	6.26	177,326	187,469	A	0.1015	In3	10	4	4	N/A
E2	1	6.26	6.26	45,573	46,371	A	0.1015	In3	10	3	3	N/A
E3	1	6.26	6.26	19,962	20,073	A	0.1015	In3	10	4	4	N/A
F	3	5.86	6.01	138	275	C	0.0762	In3	10	1	3	N/A

Table I. of experimental settings (see text for details).
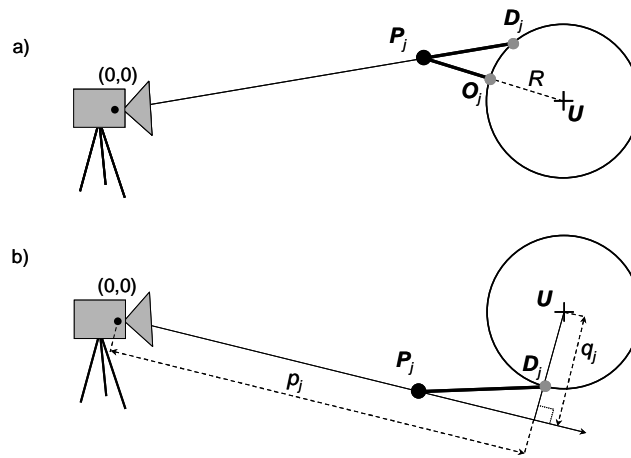
Figure 1. Geometrical interpretation of two error functions used in NLS sphere fitting: P_j is a measured point and O_j is the corresponding theoretical point for the orthogonal fitting. D_j is the corresponding theoretical point for the directional fitting when line-of-sight coming trough P_j: a) intersects with the sphere surface; b) does not intersect.
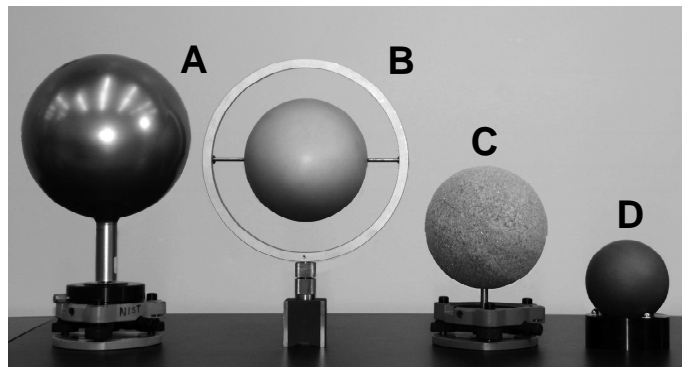

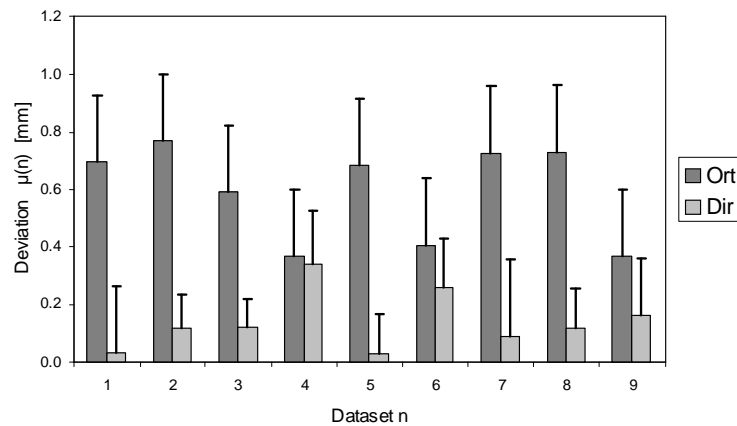Figure 2. Four spheres used in laboratory experiments (after [11]).

Figure 3. Simulated datasets: comparison of the deviations $\mu(n)$ of the fitted sphere center from the ground truth. The spheres were fitted using the orthogonal and the directional error function. Each deviation $\mu(n)$ has its own error bar determined from Equations (11), (12).
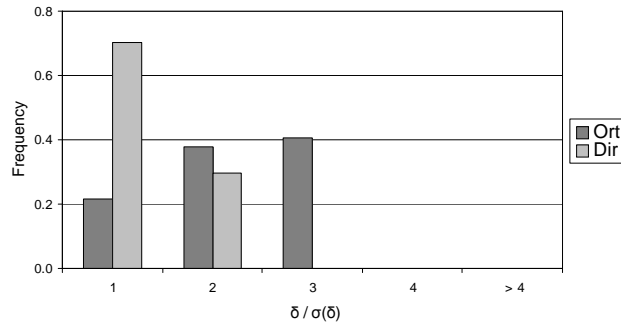
Figure 4. Simulated datasets: two histograms for orthogonal and direction fitting showing the normalized separation distances δ/σ(δ) of pairs of sphere centers.
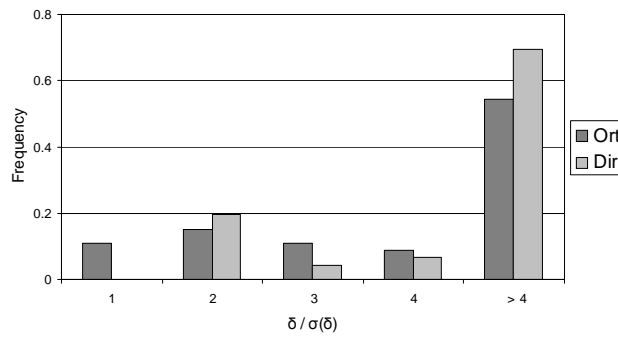
Figure 5. Lab experiments: two histograms for orthogonal and direction fitting showing the normalized separation distances δ/σ(δ) of pairs of sphere centers.
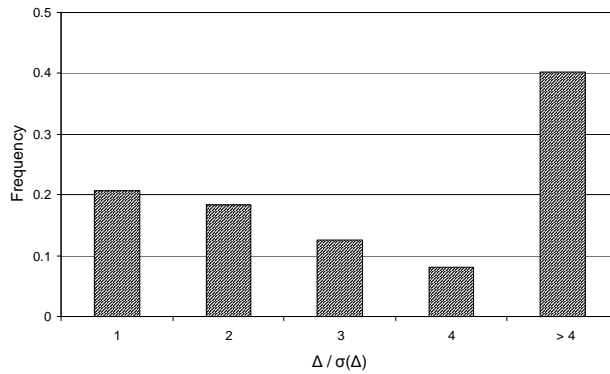

Figure 6. Lab experiments: histogram of the normalized separation distances $\Delta/\sigma(\Delta)$ between sphere centers fitted with the orthogonal and directional error functions to the same datasets.
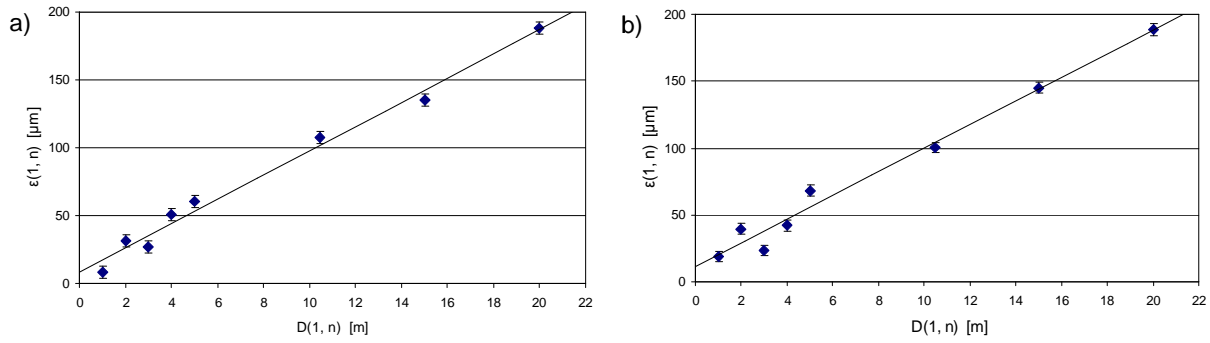
Figure 7. Lab experiments, subgroup A1: deviation ε(*1, n*) of the relative distance *D(1, n)* between the first and the *n*-th fitted sphere center from the corresponding ground truth as a function of *D(1, n)*: a) orthogonal fitting; b) directional fitting. Error bars were determined from Equations (11), (12).
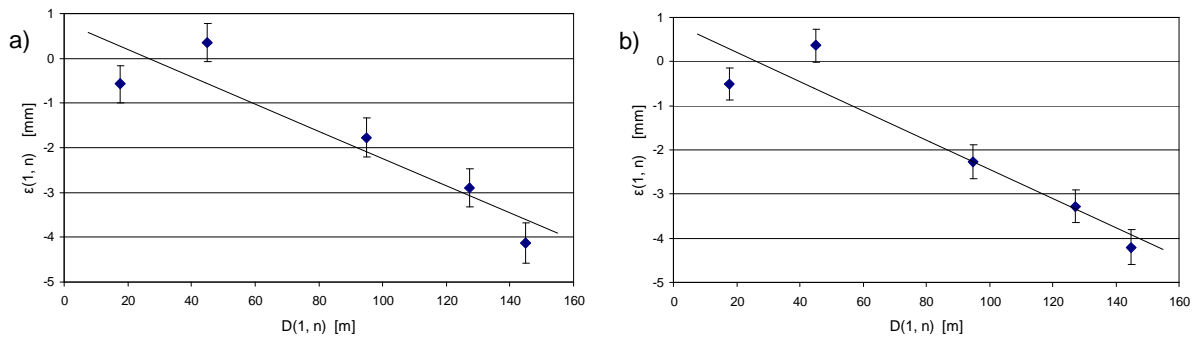

Figure 8. The same as in Figure 7 but for datasets in group B: a) orthogonal fitting; b) directional fitting.
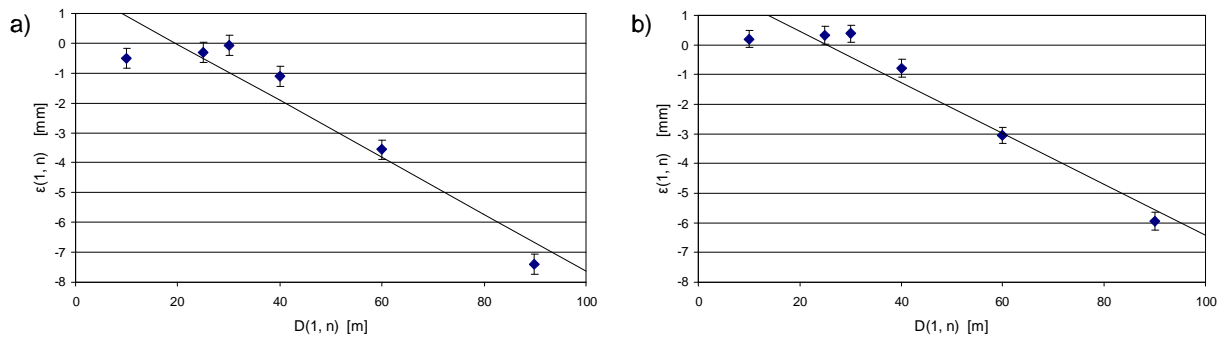

Figure 9. The same as in Figure 7 but for datasets in group C. a) orthogonal fitting; b) directional fitting.
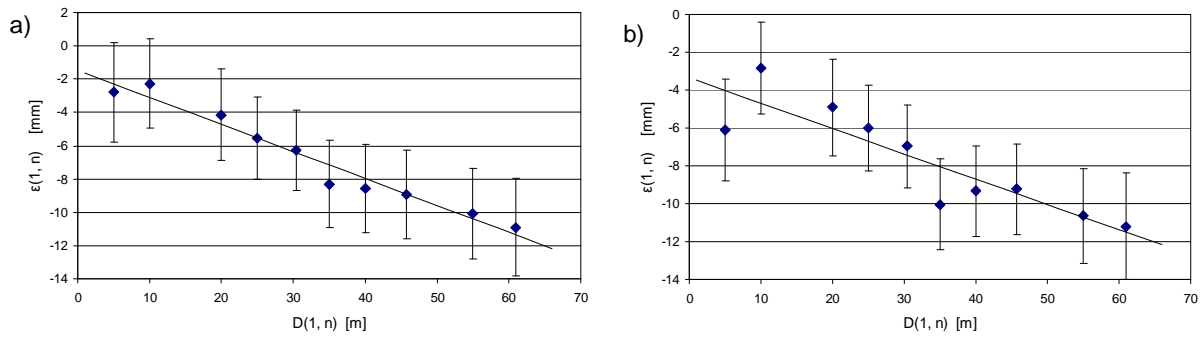
Figure 10. The same as in Figure 7 but for datasets in subgroup D2: a) orthogonal fitting; b) directional fitting. Large error bars are consequence of low scanning density and small number of data points *N*.